ACS NANO

Cite This: ACS Nano 2019, 13, 11422−11432

www.acsnano.org

ARTICLE

Broadening and Enhancing Functions of Antibodies by Self-Assembling Multimerization at Cell Surface

Lian Li,[†] Jiawei Wang,[†] Yachao Li,[†] D. Christopher Radford,[‡] Jiyuan Yang,*[,†] and Jindřich Kopeček*[,†,‡]

[†]Department of Pharmaceutics and Pharmaceutical Chemistry, Center for Controlled Chemical Delivery, University of Utah, Salt Lake City, Utah 84112, United States

[‡]Department of Biomedical Engineering, University of Utah, Salt Lake City, Utah 84112, United States

Supporting Information

ABSTRACT: **Monoclonal antibody therapy has offered treatment benefits. Nonetheless, a lack of efficacy still exists, partially because monovalent binding of antibodies to specific receptors fails to translate into an active response. Here, we report a pretargeting−postassembly approach that exploits the selective Watson−Crick base pairing properties of oligonucleotides and multivalently tethers receptor-prebound antibodies to albumin at the cell surface. We demonstrate that this two-step self-assembling strategy allows sequential actions of receptor binding and clustering that broadens and strengthens the functions of antibodies. We show that anti-CD20 obinutuzumab (OBN) modified with one morpholino oligonucleotide (OBN-MORF1) maintains the feature of naked OBN antibody upon CD20 binding, and results in actin redistribution, homotypic adhesion, and lysosome-mediated cell death. Consecutive treatment with albumin grafted with multiple copies of a complementary morpholino oligonucleotide (HSA-(MORF2)$_x$) hybridizes with surface-attached OBN-MORF1, manipulates CD20 clustering, and engages additional signals to induce calcium influx and caspase-related apoptosis. With the two types of different mechanisms collaborating in one system, the simple design exerted a notable survival extension of mice bearing disseminated B-cell lymphomas.**

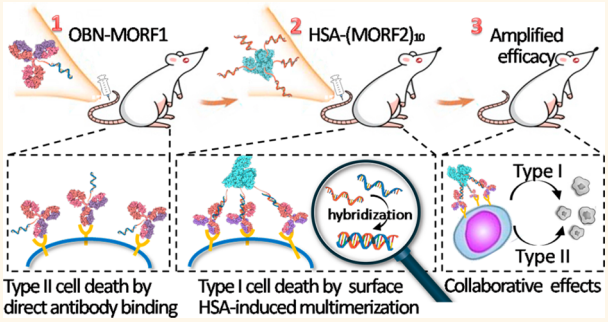

KEYWORDS: *receptor clustering, antibody assembly, morpholino oligonucleotide, human serum albumin, multivalency*

Despite the considerable success of monoclonal antibodies for cancer therapy, the therapeutic outcomes are sometimes less satisfactory.[1] Although many antibodies antagonize specific cell-surface receptors, the monovalent or divalent binding does not always elicit sufficient blockade of pro-oncogenic downstream pathways.[2−4] In many cases, it also requires those antibody-binding receptors to assemble into oligomeric complexes.[5−7] In fact, ligand-induced receptor clustering is critical for magnifying apoptosis,[8−11] and can be driven by multivalent constructs of antibodies attached to nanoparticles or polymers.[12−14] In this aspect, antibody functionalization of nanovehicles requires a defined structure with control over composition, valency, and conjugation site to ensure batch to batch reproducibility.[15] During synthesis, it is crucial to avoid the loss of antibody targeting ability and minimize the interference of its biological activity.[16] In addition, the inevitably enlarged size and the use of synthetic biomaterials might raise concerns when advancing into clinical trials. Yet, an easy, universal methodology for efficient antibody assembly at the cell surface is missing but highly demanding.

To this end, we proposed that a two-step pretargeting−postassembly approach that separates the functions of cell binding and antibody multimerization might be a cure. In this approach antibodies work independently, binding to the cell before they are triggered to self-assemble into multimers and are further endowed with increased vigor and additional functionalities. We tested this hypothesis by exploiting the selective Watson−Crick base pairing properties of oligonucleotides and using human serum albumin (HSA), a natural transport protein with long circulatory half-life, good biocompatibility for clinical practice, and multiple chemical conjugation sites,[17] to cross-link anti-CD20 antibodies.

Received: June 21, 2019
Accepted: September 25, 2019
Published: September 25, 2019

DOI: 10.1021/acsnano.9b04868
ACS Nano 2019, 13, 11422−11432

Anti-CD20 antibodies are used to treat all common B-cell hematologic malignancies, but the overall response rate is low.[18,19] Type I rituximab (RTX) binds between two CD20 tetramers resulting in accumulation in lipid rafts (cholesterol rich domains), calcium influx and caspase activation.[20] CD20 clustering by RTX itself is weak, but can be favored by its Fc interaction with Fcγ receptor on immune effector cells. However, a great proportion of patients are refractory to RTX due to the inactivity of effector cells.[20] This catalyzed the development of type II antibodies, such as obinutuzumab (OBN), which, in contrast, do not induce CD20 clustering, but instead bind within one CD20 tetramer with the conformation compatible with homotypic adhesion regions, leading to lysosome disruption and direct cell death.[21] The mechanisms of RTX and OBN are complementary, but they compete for overlapping CD20 epitopes, making their combination antagonistic.[22]

Here, we report development of a single platform that triggers two types of mechanisms of cell death induction, namely, those of type I and II anti-CD20 antibodies, and coordinates them to function collaboratively. To this end, OBN was modified with a morpholino oligonucleotide 1 (OBN-MORF1). After OBN-MORF1 pretargeted surface CD20, human serum albumin (HSA) grafted with multiple copies of complementary morpholino oligonucleotide 2 (HSA-$(MORF2)_x$) was applied as an actuator for CD20 clustering upon MORF1-MORF2 hybridization. Morpholino oligonucleotides, denoted as MORFs, have DNA bases attached to an altered backbone of methylenemorpholine rings linked through phosphorodiamidate groups. In comparison to DNA molecules, complementary MORFs also form double helices by Watson–Crick base pairing (hybridization), but their charge-neutral phosphorodiamidate backbone endows them with much stronger binding affinity than DNA, and makes them more biocompatible and nuclease resistant, which ensures *in vivo* stability and safety. We hypothesized that following OBN-MORF1 binding to CD20, receptor cross-linking bridged by HSA-$(MORF2)_x$ would impose type I properties to type II antibodies and create a therapeutic that combines effects of both antibody types, producing greater antitumor activity (Scheme 1).

Scheme 1. Pretargeting–Postassembly Approach That Assembles OBN Antibodies at Cell Surface[a]

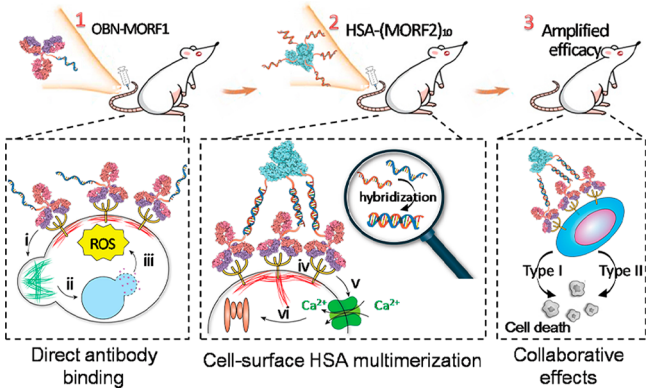

[a]Without compromising the original effects of (i) actin remodeling, (ii) lysosome disruption, and (iii) ROS production afforded by naked OBN upon direct cell binding, clustered OBN after HSA-mediated multimerization simultaneously induces additional effects of (iv) receptor cross-linking, (v) calcium influx, (vi) caspase activation, which confers complementary mechanism to enhance apoptosis.

RESULTS AND DISCUSSION

Synthesis and Characterizations. To synthesize antibody-MORF1, whole antibody of RTX and OBN were partially reduced to selectively expose the thiol groups in the hinge region leaving the Fab′ region available for receptor binding, followed by the thiol–ene reaction with maleimide-functionalized MORF1 (Figure 1A). Similarly, multivalent HSA-$(MORF2)_x$ was generated *via* the thiol–ene reaction between freshly reduced MORF2 (3′-primary terminated with thiol group) and maleimide-functionalized HSA (Figure 1B). The conjugates with defined structures were confirmed by the single peaks that shifted toward smaller elution volumes in size-exclusion chromatography as molecular weight increased with successful attachments of morpholino oligonucleotides. These conjugates were further characterized using bicinchoninic acid protein assay determining antibody or HSA concentrations, UV–vis spectrophotometry determining MORF concentrations, gel electrophoresis, and mass spectroscopy; see Table 1 and Supporting Information Figures S1–S3.

As illustrated in Figure 1C, both OBN-MORF1 and HSA-$(MORF2)_{10}$ were initially less than 10 nm in diameter, whereas their mixture at 1:1 MORF1:MORF2 ratio resulted in substantial increase in size (~40 nm), indicating their self-assembly. To validate that MORF1-MORF2 biorecognition triggered the hybridization of the two conjugates, "hypochromic effect", in which hydrogen bonding between complementary bases in MORFs decreases the resonance of the aromatic rings,[23] was evaluated. As shown in Figure 1D, the optical density at 260 nm of their mixture in phosphate buffered saline (PBS, pH 7.4) dropped to a minimum when MORF1 and MORF2 were in equimolar amounts. Meanwhile, incubation in 0.1 N hydrochloric acid (HCl) that destroyed the MORF1-MORF2 interaction prevented the "hypochromic effect", and resulted in the collapse of OBN-MORF1 and HSA-$(MORF2)_{10}$ aggregates. In addition, the efficient hybridization between these two conjugates *via* specific biorecognition between MORF1 and MORF2 was further confirmed by gel electrophoresis (Supporting Information Figure S3).

Two-Step Binding at Cell Surface. In this general approach, cell-surface multimerization of antibodies requires two sequential steps: (i) specific receptor binding *via* antibody targeting, and (ii) multivalent attachment to HSA *via* MORF1-MORF2 hybridization. Thus, to demonstrate the self-assembly of antibody-MORF1 and HSA-$(MORF2)_x$ at surface CD20, a coculture of CD20 positive Raji-GFP (expressing green fluorescent protein) and CD20 negative DG-75 cells were consecutively exposed to Cy5-labeled RTX-MORF1/OBN-MORF1 and Cy3-labeled HSA-$(MORF2)_x$. As shown in Figure 2A, majority of Raji-GFP cells were dual stained with Cy3 and Cy5, while DG-75 cells had minimum fluorescence, demonstrating that the system is highly CD20 specific. Moreover, a profoundly stronger signal of Förster resonance energy transfer (FRET), which was generated by the close proximity of Cy5 to Cy3, was observed in Raji-GFP cells than DG-75 cells, indicating that the first step of receptor binding is the prerequisite for the next step of surface biorecognition between antibody-MORF1 and HSA-$(MORF2)_x$.

To visualize the self-assembly on cell surface, Raji B cells were pretreated with OBN-MORF1-Cy5 or RTX-MORF1-Cy5, followed by sequential exposure to HSA-$(MORF2)_{10}$-Cy3. As expected, the cell membrane was decorated with a

DOI: 10.1021/acsnano.9b04868
ACS Nano 2019, 13, 11422–11432

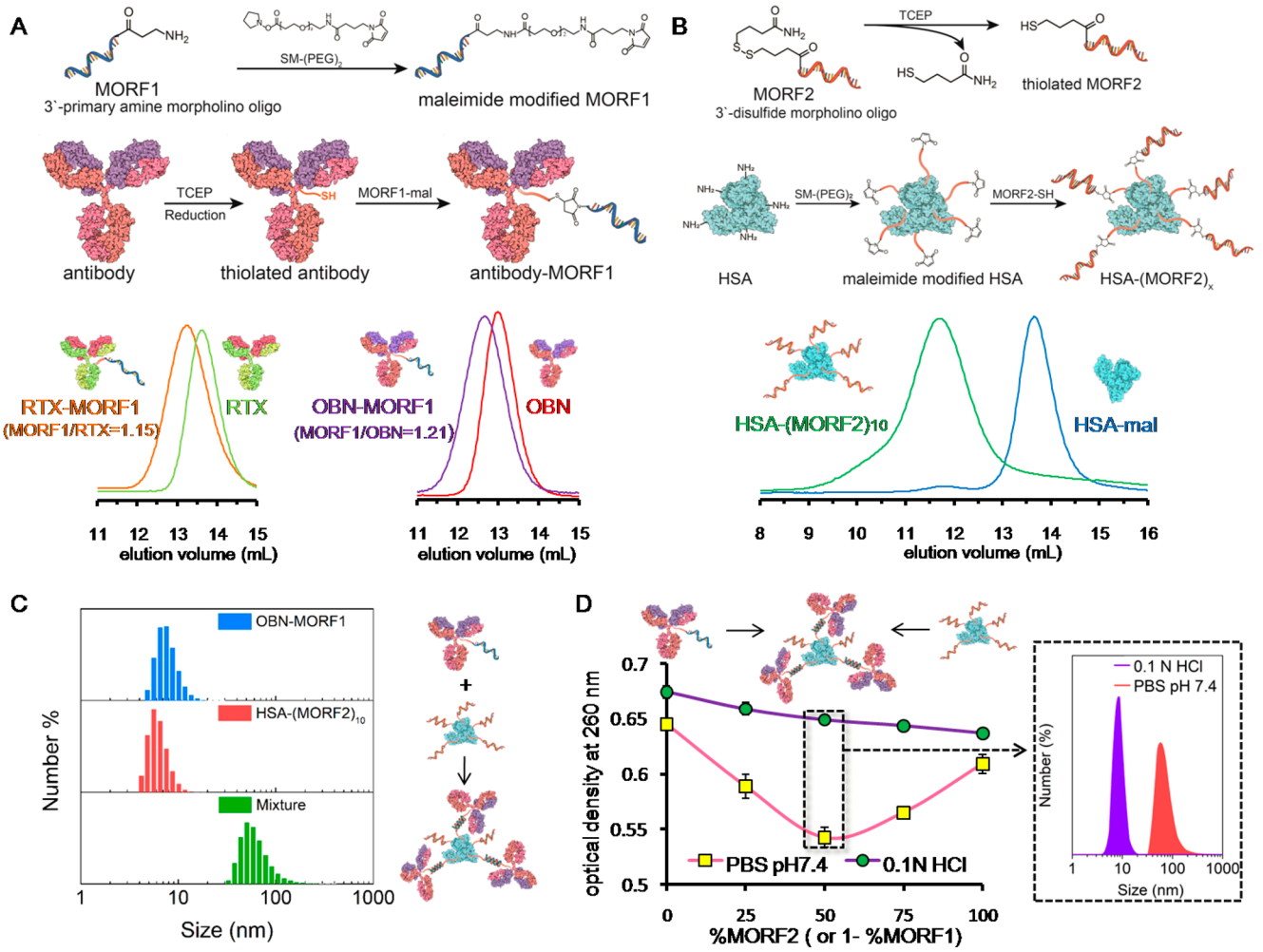

Figure 1. Illustration of synthesis and size-exclusion chromatography characterization of (A) antibody (RTX or OBN)-MORF1 conjugates and (B) HSA-(MORF2)$_x$ conjugates as determined on Superdex 200 10/300 GL column eluted with PBS (pH 7.2) at flow rate 0.4 mL/min and UV wavelength 280 nm. (C) Dynamic light scattering of the two conjugates and their mixture (equimolar MORF1/MORF2) in pH 7.4 PBS. (D) Hypochromic effect upon hybridization between the two conjugates when they were mixed in different ratios, as measured by the optical density at 260 nm in PBS pH 7.4 or 0.1 N HCl solution.

Table 1. Conjugate Characterization

conjugate	MORF valence	Cy5/antibody	Cy3/HSA
RTX-MORF1	1.15	–	–
RTX-MORF1-Cy5	1.12	1.74	–
OBN-MORF1	1.21	–	–
OBN-MORF1-Cy5	1.18	1.65	–
HSA-MORF2	1.2	–	–
HSA-(MORF2)$_5$	5.4	–	–
HSA-(MORF2)$_{10}$	9.4	–	–
HSA-(MORF2)$_{15}$	16.6	–	–
HSA-(MORF2)$_{10}$-Cy3	11.4	–	1.46

substantial colocalization of Cy3 and Cy5 fluorescence (Figure 2B). In addition, when antibody-MORF1-Cy5 pretargeted cells were further incubated with a mixture of HSA-(MORF2)$_{10}$-Cy3 and excessive free MORF2, the binding of HSA onto cells was drastically reduced (Figure 2C), indicating the cell-surface tethering of antibody to HSA *via* MORF1-MORF2 interaction.

Surface Assembling of Antibodies Amplifies Apoptosis. We next evaluated whether clustering CD20-bound antibodies by albumin further amplified apoptosis (Figure 3). We coined the term "clustered OBN/RTX" (cOBN/cRTX) to describe the consecutive treatment composed of OBN-MORF1/RTX-MORF1 followed by HSA-(MORF2)$_x$. As shown in Figure 3A, HSA-(MORF2)$_{10}$ alone did not contribute to cytotoxicity, as compared with the untreated group. Although RTX binds between two CD20 tetramers,[20] its capability to bivalently cross-link CD20 was insufficient and only led to moderate apoptosis. Clustered RTX-MORF1 by multivalent HSA-(MORF2)$_{10}$ (cRTX) resulted in an increased level of early apoptosis because of the amplification of surface CD20 cross-linking. Meanwhile, even binding within one CD20 tetramer,[22] OBN itself could trigger potent apoptosis (especially late apoptosis). By comparison, the addition of RTX (RTX+OBN) antagonized the efficacy of OBN, most likely due to the mutual interference during competing for binding their overlapping CD20 epitope.[22] In contrast, cell-surface clustering of OBN-MORF1 by HSA-(MORF2)$_{10}$ (cOBN) further enhanced the OBN-triggered induction of apoptosis, leading to substantial cell death significantly higher than all controls.

To gain insight into the influence of the conjugates' structure on apoptosis induction, we investigated the effect of HSA-(MORF2)$_x$ valence, and compared the whole OBN antibody with its Fab′ fragment. Figure 3B shows the

DOI: 10.1021/acsnano.9b04868
ACS Nano 2019, 13, 11422−11432

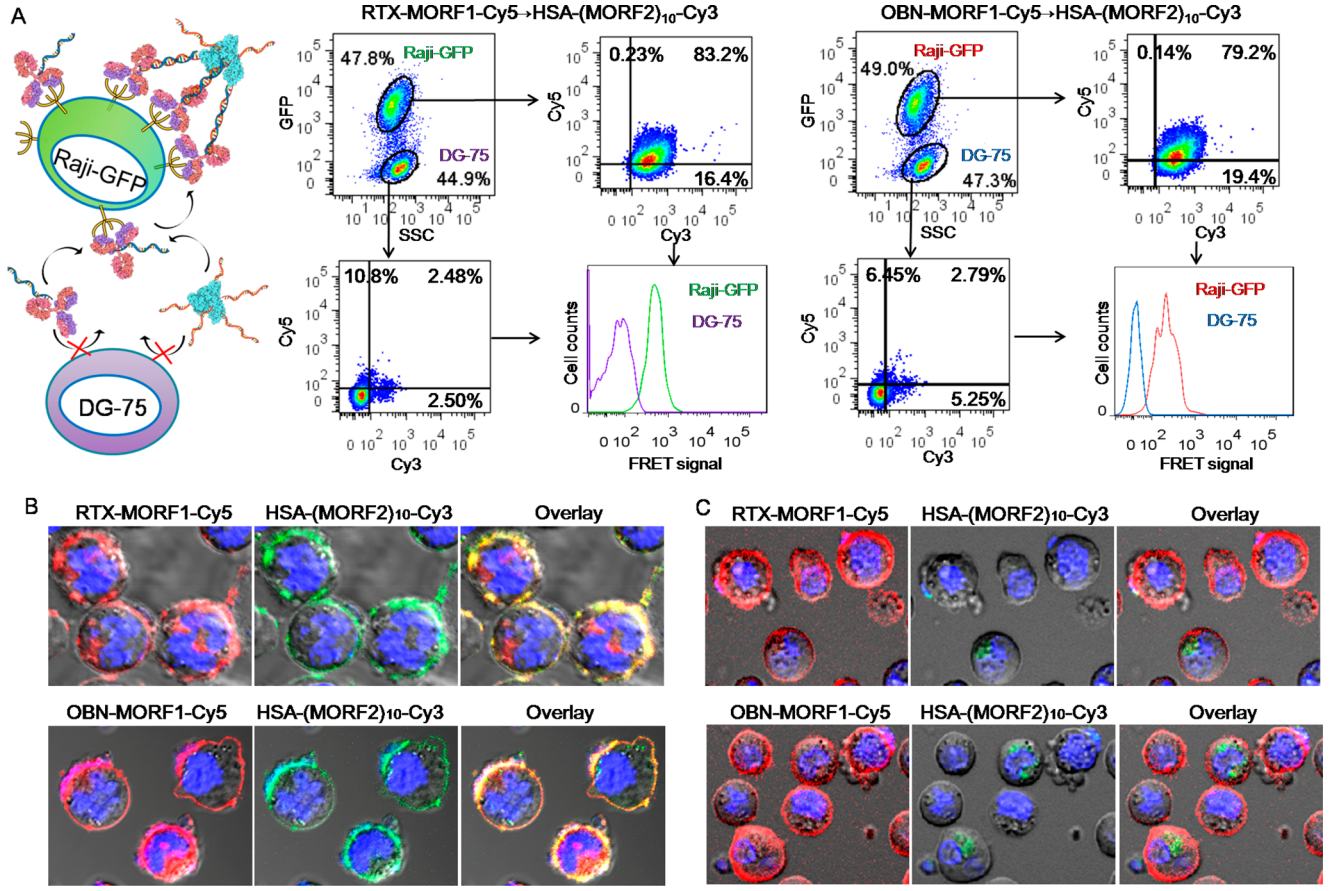

Figure 2. (A) The highly specific self-assembly of antibody-MORF1 and HSA-$(MORF2)_x$ at the surface of CD20 expressing Raji B cells. A coculture of CD20 positive Raji-GFP cells and CD20 negative DG-75 cells with 1:1 ratio were exposed to 0.5 μM Cy5-labeled RTX-MORF1 or OBN-MORF1 for 1 h. Afterward, cells were washed to remove the unbound conjugates and further incubated with Cy3-labeled HSA-$(MORF2)_{10}$ (0.5 μM MORF2) for another 1 h. Fluorescence of Cy5, Cy3, and their FRET signal in different cells (distinguished by GFP expression) was analyzed by flow cytometry. Confocal microscopic images of antibody-MORF1-Cy5 pretreated Raji cells after consecutive treatment with HSA-$(MORF2)_{10}$-Cy3 in the (B) absence or (C) presence of excessive free MORF2 (20 μM). Red: Cy5; Green: Cy3; Blue: nuclei.

multivalency of HSA-$(MORF2)_x$ is essential for cRTX and cOBN-augmented apoptosis. In contrast to HSA-$(MORF2)_x$ conjugate, which functions as cross-linking effector and largely relies on MORF2 multivalence, OBN-$(MORF1)_3$ conjugate with higher MORF1 valence showed slightly decreased induction of apoptosis as compared with monovalent OBN-MORF1, after HSA-$(MORF2)_{10}$ cross-linking (Supporting Information Figure S4). This might be explained in the following way: Once one MORF1 recognizes MORF2, the extra MORF1 motifs on the same antibody are more prone to hybridize and consume the MORF2 motifs on HSA-$(MORF2)_x$ conjugate, which decreases the ability of HSA-$(MORF2)_x$ to accommodate other OBN-$(MORF1)_x$; consequently, the cross-linking effect of CD20 receptors is compromised, resulting in decreased apoptosis induction.

Notably, multivalent cross-linking of Fab′ fragment from OBN (Supporting Information Figure S5) was not effective to further enhance apoptosis (Figure 3C). This suggests the importance of binding orientation toward CD20 and the elbow angle of OBN to elicit direct cell death.[22] Consistent with numerous studies,[22,24] the maximum binding to CD20 showed that OBN occupied only half of the number of CD20-binding sites as RTX (Figure 3D). This could be explained by the inter-CD20 tetramer binding of type I RTX, resulting in two antibodies bound per tetramer, and intratetramer binding of type II OBN, resulting in only one antibody bound per CD20 tetramer. Interestingly, Fab′$_{(RTX)}$-MORF1 and Fab′$_{(OBN)}$-MORF1 showed similar CD20 binding curves (Figure 3D), suggesting converting whole OBN antibody to Fab′ abrogated that specific conformation, and the type II specific functions were lost. In contrast, clustered cOBN triggered higher apoptosis than naked OBN, indicating CD20 cross-linking might give additional mechanism to type II antibody to kill B cells.

cOBN Combines Type I and Type II Effects. CD20 redistribution in lipid rafts is a typical characteristic of type I anti-CD20 antibody, which subsequently triggers calcium influx and a series of downstream pathways.[25] We are aware of discrepancies in the literature on the existence of lipid rafts.[26,27] The results below are discussed using the term "lipid rafts" but could also be interpreted using "cholesterol rich membrane domains".

As shown in Figure 4A, a great proportion of RTX bound on cell surface and redistributed within lipid rafts. A further increment in lipid raft colocalization occurred when cells were treated with cRTX, because cRTX augmented surface CD20 cross-linking. Unlike type I RTX, OBN induced strong homotypic cell aggregation, massively accumulated at cell−cell contact sites, and did not substantially translocate into lipid rafts, which are typical type II characteristics.[21] Of note, cOBN

DOI: 10.1021/acsnano.9b04868
ACS Nano 2019, 13, 11422−11432

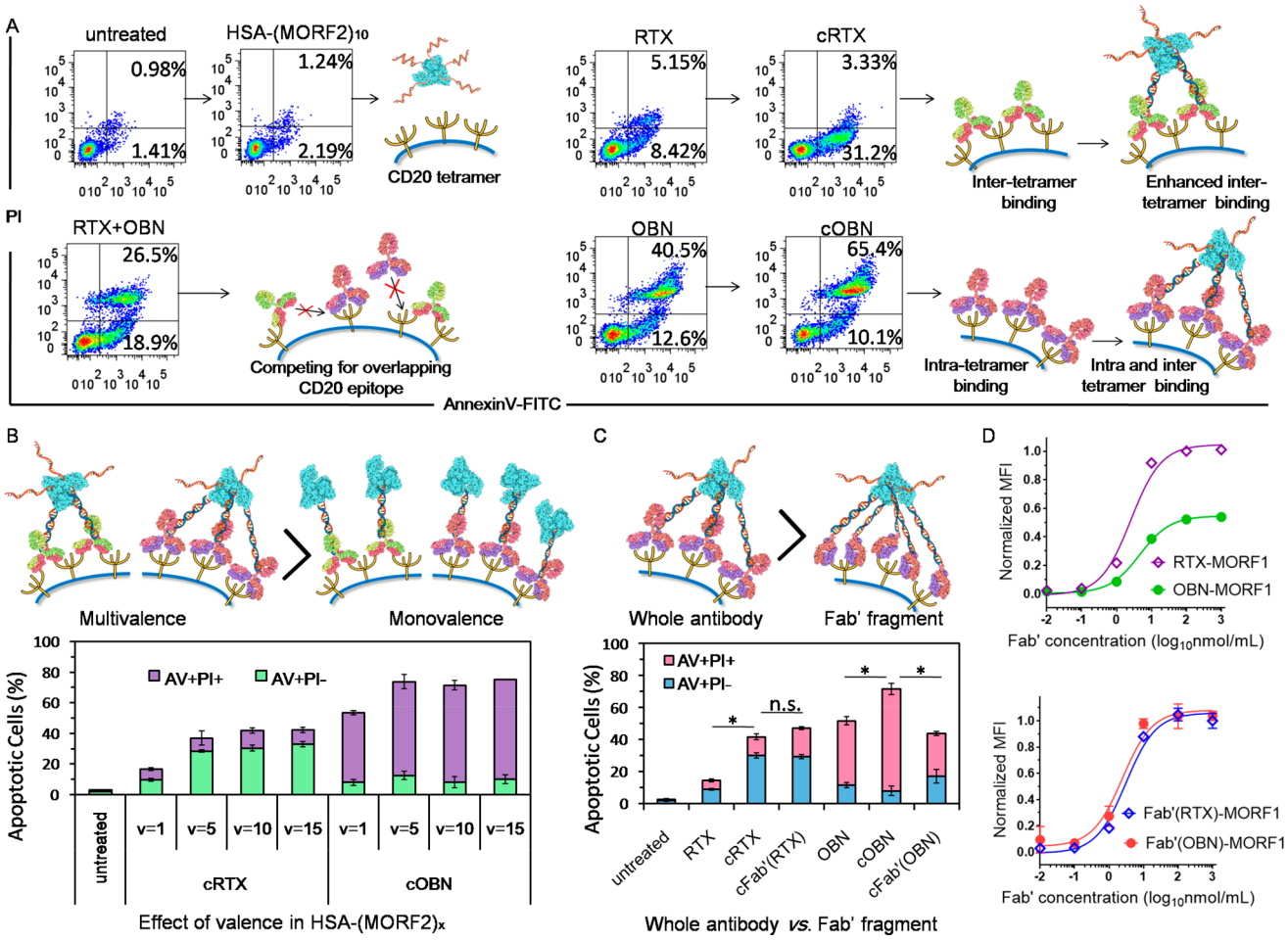

Figure 3. (A) Apoptosis induction in Raji cells untreated or treated with RTX, cRTX, OBN, cOBN, or combination of RTX and OBN. (B) Effects of valency of HSA-$(MORF2)_x$ on cRTX/cOBN mediated apoptosis induction. (C) Comparison of whole antibody and Fab′ fragment after multivalent attachment to HSA-$(MORF2)_{10}$ to induce apoptosis. (D) CD20 binding assay comparing maximum binding of RTX-MORF1, OBN-MORF1, Fab′(RTX)-MORF1, and Fab′(OBN)-MORF1 to Raji cells. *$P < 0.05$, n.s., not significant, by Student's t test.

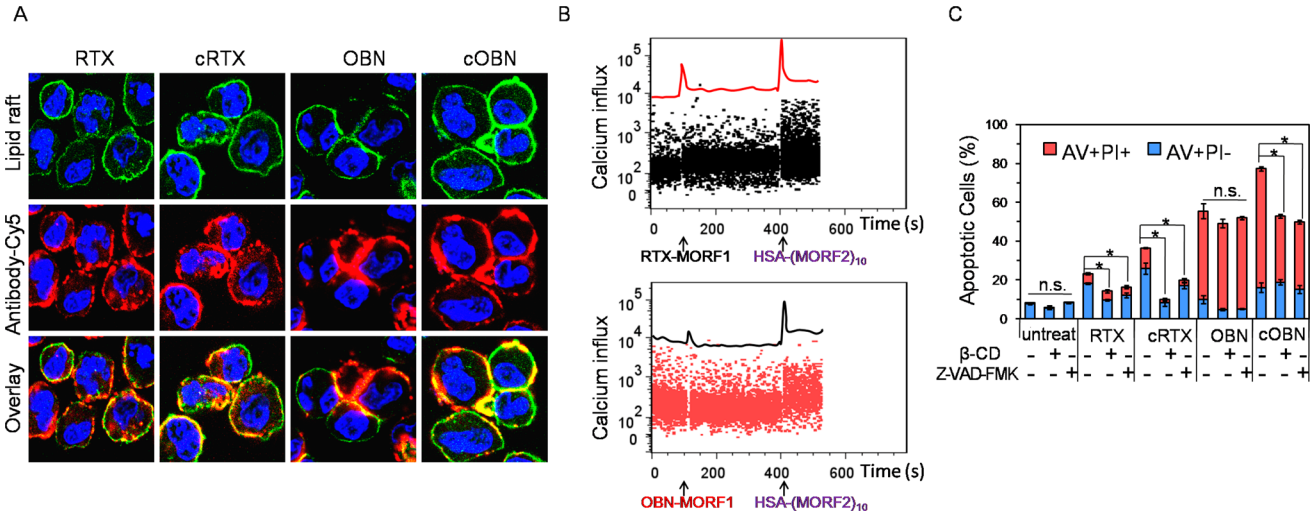

Figure 4. Apoptotic pathways including (A) CD20 redistribution in lipid rafts, (B) calcium influx, and (C) caspase activity after Raji cells were treated with RTX, cRTX, OBN, or cOBN. *$P < 0.05$, n.s., not significant, by Student's t test.

not only induced homotypic cell aggregation but also substantially colocalized with lipid rafts, indicating cOBN had characteristics of both type I and type II anti-CD20 antibodies. As shown in Figure 4B, before HSA-$(MORF2)_{10}$ stimulation, RTX-MORF1 mediated moderate calcium influx while OBN-MORF1 did not induce calcium influx. This is because RTX binds between CD20 tetramers resulting in redistribution in lipid rafts, and OBN binds within one

DOI: 10.1021/acsnano.9b04868
ACS Nano 2019, 13, 11422−11432

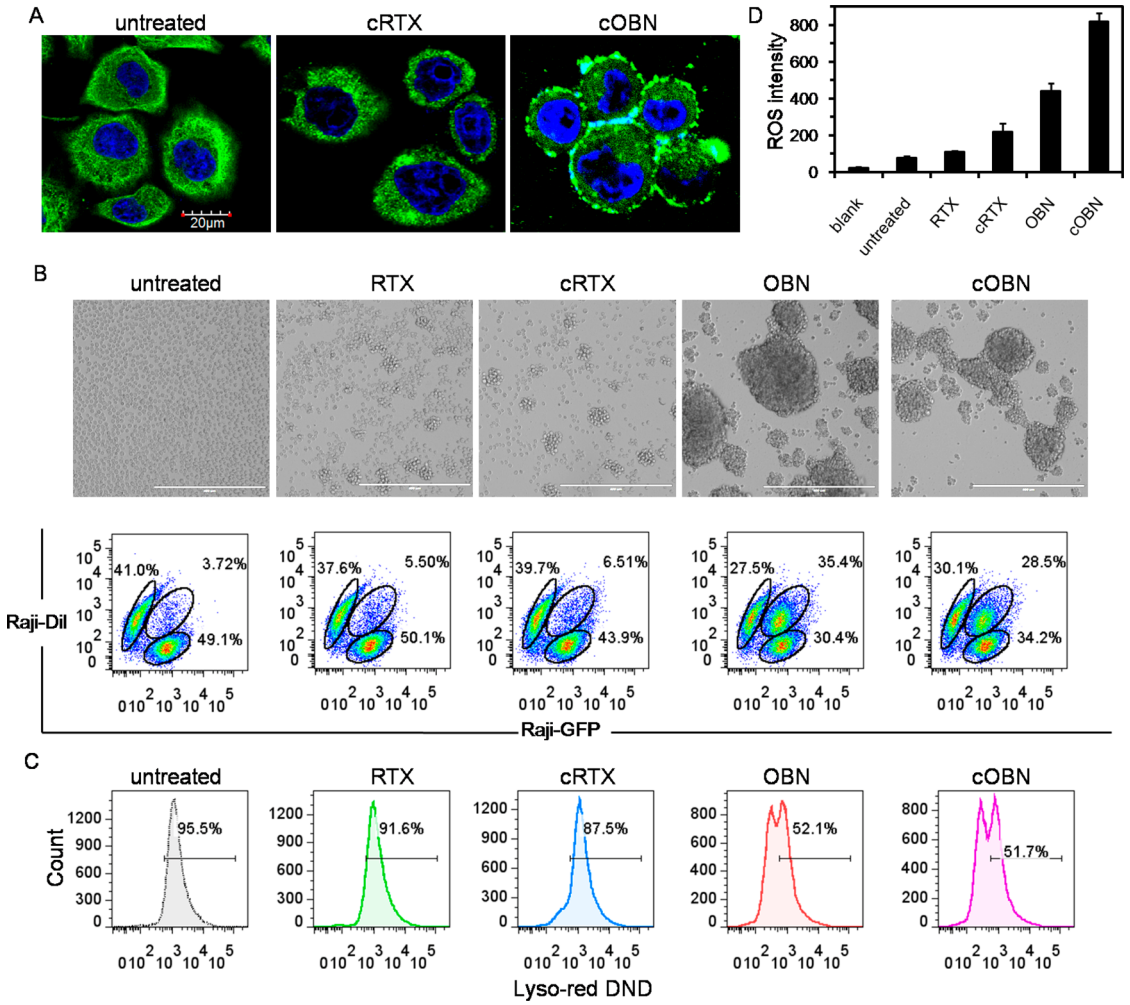

Figure 5. Type II apoptotic pathways including (A) actin cytoskeleton remodeling, (B) intercell homotypic adhesion, (C) lysosome-mediated cell death, and (D) ROS generation after Raji cells were treated with RTX, cRTX, OBN, or cOBN.

tetramer without involvement of CD20 cross-linking.[22] Interestingly, after HSA-$(MORF2)_{10}$ stimulation, a significant rise in calcium concentration occurred for both RTX-MORF1 and OBN-MORF1, which could be explained by the multivalent binding by HSA-$(MORF2)_{10}$ recognition and subsequent surface CD20 clustering. To further investigate whether CD20 cross-linking and caspase activation were involved in cRTX/cOBN-induced apoptosis, Raji cells were pretreated with β-cyclodextrin (β-CD) to deplete cholesterol[28,29] or pan caspase inhibitor Z-VAD-FMK, followed by the various treatments. Figure 4C shows CD20 clustering and caspase activation were engaged in RTX and cRTX treatments, but not involved in OBN treatment. Notably, cOBN exploited both type I and type II mechanisms and gave additional apoptosis induction as compared with OBN.

cOBN also maintained typical type II characteristics, resulting in the enrichment of F-actin at cell surface and cell−cell adhesion sites (Figure 5A), pronounced intercell homotypic adhesion (Figure 5B), and disrupted lysosomes (Figure 5C), while cRTX's influence was weak and limited. Reactive oxygen species (ROS) are generated downstream of OBN-induced actin cytoskeletal reorganization and lysosome membrane permeabilization, and play a central role in inducing potent cell death.[30] RTX could also contribute to ROS production by causing mitochondrial depolarization.[31] Thus, ROS production is related to the shared downstream pathways by both type I and type II antibodies. As demonstrated in Figure 5D, RTX only mediated modest ROS production as compared with the untreated control, while cRTX greatly increased the level of ROS generation due to the amplified CD20 clustering and subsequently higher level of mitochondrial depolarization. Meanwhile, OBN significantly augmented the ROS production because lysosome disruption directly induces potent ROS evocation.[30] Moreover, a further enhancement in ROS generation was induced when Raji cells were treated with cOBN. This might be the consequence of involvement of both type I and type II pathways.

***In Vivo* Validation of cOBN Activity.** Having demonstrated cOBN combines the effects of type I and type II anti-CD20 antibodies, we sought to test its therapeutic efficacy *in vivo*. NOD/SCID-Rag1$^{null}\gamma^{null}$ (NRG) mice bearing systemically disseminated Raji B-cell lymphomas were given three doses of saline, OBN, and cOBN weekly as indicated in Figure 6A. Saline treated mice became hind limb paralyzed rapidly with the median survival of 19 days. OBN significantly extended the median survival to 57 days. Significantly, cOBN further prolonged the mice survival with the median survival of 83 days, and half of the mice were still paralysis-free after 100 days (Figure 6B) without the loss of body weight (Figure 6C). At the end point, bone marrow (BM) cells were isolated from

DOI: 10.1021/acsnano.9b04868
ACS Nano 2019, 13, 11422−11432

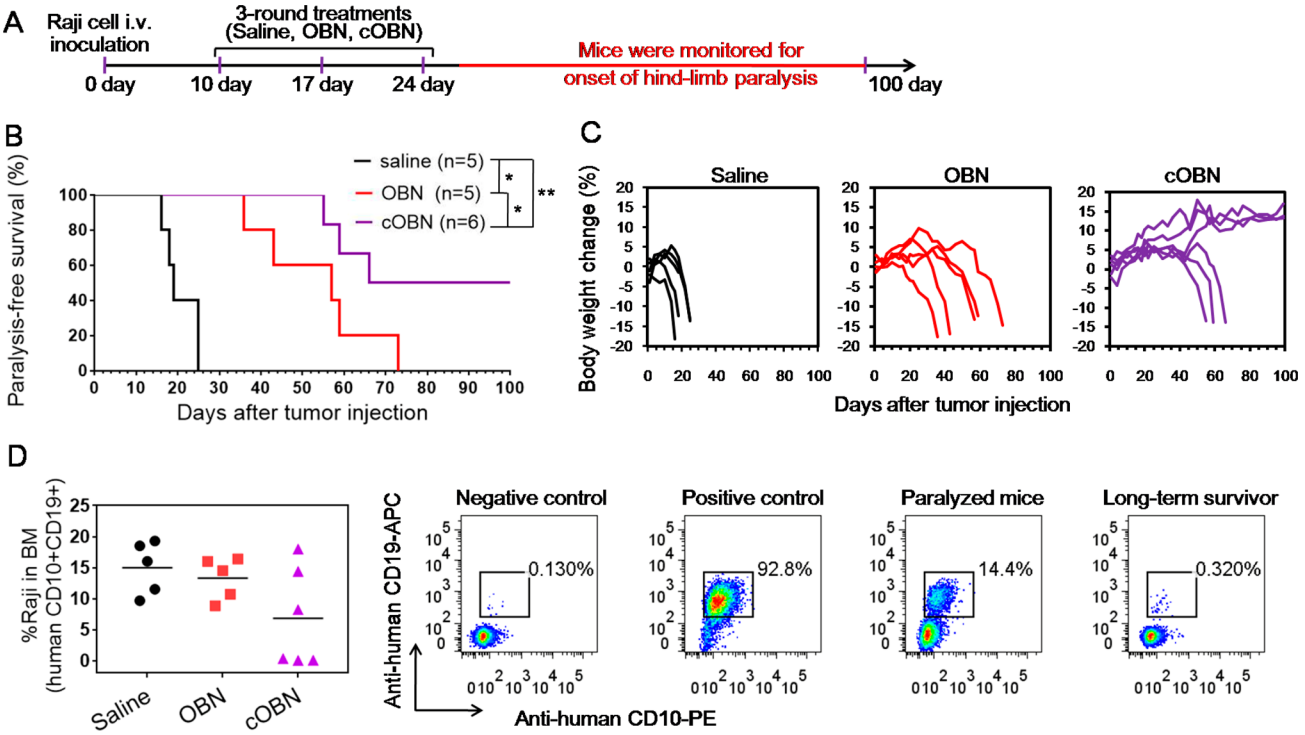

Figure 6. (A) Treatment schedule (see Experimental Procedures for dosing), (B) paralysis-free survival, (C) body weight change, and (D) residual Raji cells (human CD10+CD19+) in bone marrow (BM) of NRG mice bearing disseminated Raji B-cell lymphomas after treatment with saline, OBN, or cOBN. A 5 h interval was applied between the consecutive injections of OBN-MORF1 and HSA-$(MORF2)_{10}$ for cOBN treatment. BM cells isolated from native NRG mouse served as the negative control, and Raji cells served as the positive control. *$P < 0.05$, **$P < 0.01$, by Student's t test.

femur, and dissemination of Raji cells (human CD10+CD19+) in BM was analyzed (Figure 6D and Supporting Information Figure S6). Variably significant amounts of Raji cells were observed in BM of paralyzed mice from different treatments. However, in long-term survivors treated with cOBN, the presence of Raji cells was minimal.

Previously, we demonstrated that multivalent cross-linking of CD20-pretargeted Fab′ fragments from RTX by *N*-(2-hydroxypropyl)methacrylamide (HPMA) copolymer amplified apoptosis and circumvented numerous resistant pathways.[8,23] While still exploiting the concept of two-step pretargeting–postassembly, the next-generation platform developed herein has several features, which leads to broader impacts in the following aspects.

First, it broadens the scope of application. Previous strategies harnessed Fab′ fragments of antibodies solely as targeting agents, and primarily focused on augmenting the cross-linking of surface receptors. The application is limited to antibodies that activate a similar pathway (receptor ligation) to induce apoptosis, such as RTX. In contrast, due to the loss of antibody conformation and abrogation of initial effect, such approach is not applicable to a variety of antibodies whose main mechanisms of action exclude receptor cross-linking. This is exemplified by our results that hyper-cross-linking of OBN Fab′ failed to further improve results obtained with OBN (Figure 3C). Instead, the current strategy switches the focus to cell-surface multimerization of antibodies, which looks to its application in a broader range. To this end, Fab′ fragment is replaced by whole antibody. As for the case of cOBN, it not only simplifies the fabrication process, but also brings the benefits of antibody multimerization at the cell surface receptor (Figure 4) while still maintaining the biological activities of the original antibody (Figure 5). This eventually leads to a significant enhancement in therapeutic efficacy (Figure 3A and 6).

Second, it broadens the functions of the antibody. The mechanisms of type I and type II anti-CD20 antibodies are distinct and theoretically complementary, but in reality their combination is antagonistic because their binding epitopes overlap. Our two-step strategy spatially separates the operations of receptor binding by OBN-MORF1 pretargeting (exerting type II effects) and antibody multimerization by HSA-$(MORF2)_x$ cross-linking (exerting type I effects), which ensures them to work independently. As compared with a previous strategy that largely relied on amplification of type I signals, the next generation combines the activation pathways of type I and type II antibodies into one system. In our previous study using HPMA copolymer (P-$(MORF2)_x$ conjugate) to cross-link Fab′$_{(RTX)}$-MORF1 pretargeted cells, direct stochastic optical reconstruction microscopy (dSTORM) indicated sporadic cell-to-cell cross-linking.[32] With a more rigid structure of HSA in the current study, the ability of HSA-$(MORF2)_x$ to accommodate OBN-MORF1 attached on the same cell might decrease. However, the pretreatment of type II OBN antibody induces significant cell aggregation. The consequently closer proximity between cell interfaces is highly likely to increase the chance for unoccupied MORF2 in HSA-$(MORF2)_x$ to hybridize with OBN-MORF1 bound to other cells. Thus, intracell and intercell CD20 cross-linking might simultaneously occur after cOBN treatment. This approach might further provide additional treatment strategies suitable for a broader spectrum of B-cell malignancies, including treatment-resistant tumors.

DOI: 10.1021/acsnano.9b04868
ACS Nano 2019, 13, 11422−11432

Third, it broadens the utilization of the technique. In addition to random-coiled HPMA copolymers-MORF2 conjugates that were previously used for CD20 cross-linking, we demonstrated a more rigid structure of HSA-$(MORF2)_x$ (x = 5, 10, 15) with multivalency hybridized with antibody-MORF1 and effectively induced significant apoptosis (Figure 3B). This implies that this technique is general and can be expanded to various nanovehicles ranging from linear polymers to more rigid systems (*e.g.*, proteins, nanoparticles, micelles). Moreover, HSA is a natural transport protein with a long circulatory half-life, natural biocompatibility, and multiple ligand binding sites. It is already an effective carrier for drugs, peptides, and antibodies in clinical applications, with good reproducibility, large-scale manufacture capability, and low cost. As compared with the original effector using HPMA copolymer, the HSA-based construct has its own advantage in translatability into clinics.

CONCLUSIONS

In summary, we successfully multimerized and cross-linked CD20-prebound OBN antibody by exploiting the hybridization of a pair of complementary oligonucleotides and tethering antibodies to HSA. Normally, type I and type II anti-CD20 antibodies exploit complementary mechanisms of cell death induction to treat B-cell malignancies, but their combination is antagonistic. Our designed system provides a therapeutic approach capable of maintaining the characteristic features of type II antibodies and simultaneously inducing additional type I effects: OBN-MORF1 targets CD20, leading to actin cytoskeleton remodeling, lysosome disruption, and ROS production; HSA-$(MORF2)_{10}$ cross-links CD20-bound OBN-MORF1, resulting in calcium influx and caspase activation. With the two types of mechanisms collaborating in one system, cOBN (OBN-MORF1 followed by HSA-$(MORF2)_x$) showed notable survival extension of mice bearing disseminated Raji B-cell lymphomas. As antibodies, oligonucleotides, and HSA are all clinically used and commercially available, we expect our simple but rational two-step pretargeting−postassembly strategy for multimerizing antibodies at the cell surface may be easily expanded to arm other antibodies targeting different receptors with additional functionalities and strengthen their therapeutic efficacy.

EXPERIMENTAL SECTION

Synthesis of Antibody-MORF1 Conjugate. First, the end amino group of 3′-amine-derivatized 25-mer phosphorodiamidate morpholino oligomer MORF1 (5′-GAGTAAGCCAAGGAGAATCA-ATATA-linker-amine-3′, MW = 8630.5 Da, customized and purchased from Gene Tools, Philomath, OR) was converted to maleimide group by the reaction with 50 excess of succinimidyl-(*N*-maleimidopropionamido)-diethylene glycol]ester (SM-$(PEG)_2$, Thermo Fisher Scientific). Briefly, 3′-amine-derivatized MORF1 (1.8 mg, 200 nmol) was dissolved in 100 μL of 10 mM phosphate buffered saline (PBS, pH 7.4), and SM-$(PEG)_2$ (4.25 mg, 10 μmol) was dissolved in 50 μL of dimethyl sulfoxide. Then the two solutions were mixed and the reaction was stirred for 2 h at room temperature to produce maleimide modified MORF1. Afterward, unreacted SM-$(PEG)_2$ was removed by ultracentrafiltration (Ultracel 3000 Da MWCO, Millipore) with 10 mM PBS (pH 6.5) washing four times. Maleimide content was measured using modified Ellman's assay, and >90% conversion was achieved.

To conjugate MORF1 to monoclonal antibody rituximab (RTX) or obinutuzumab (OBN), RTX (Genentech) or OBN (Genentech) with the concentration of 4 mg/mL was reduced by 20 mM tris(2-carboxyethyl)phosphine (TCEP, Sigma-Aldrich) in 100 mM citric buffer (pH 5.5) at 37 °C for 2 h to selectively expose the thiol group in the hinge region.[33] Afterward, the reduced antibodies were purified by ultracentrafiltration (Ultracel 30 000 Da MWCO, Millipore) with 10 mM PBS (pH 6.5) four times. Ellman's assay was used to quantify the amount of exposed thiol groups on antibodies, and approximately ∼6 thiol groups were found on a single thiolated RTX and thiolated OBN. The conjugation of maleimide modified MORF1(300 μM) to thiolated RTX/OBN (200 μM) was performed in 0.5 mL of 10 mM PBS (pH 6.5) at room temperature for 2.5 h with the feeding molar ratio [MORF1]:[RTX/OBN] of 1.5:1. The fabricated RTX-MORF1 and OBN-MORF1 was further purified by ultracentrafiltration (Ultracel 30 000 Da MWCO, Millipore) with 10 mM PBS (pH 7.4) washing four times.

To prepare fluorescent-labeled RTX-MORF1-Cy5 and OBN-MORF1-Cy5, the lysine side-chains of RTX and OBN (4.5 mg, 30 nmol) were reacted with cyanine 5 monosuccinimidyl ester (Cy5-NHS, Lumiprobe, 40 μg, 60 nmol) in 1 mL PBS (pH 7.4) for 2 h at room temperature with the feeding molar ratio [antibody]:[Cy5-NHS] of 1:2. The obtained RTX-Cy5 and OBN-Cy5 was further purified using a PD 10 column to remove the unreacted dye, then reduced by TCEP to expose thiol groups and conjugated with maleimide modified MORF1 as described above.

Synthesis of HSA-$(MORF2)_x$ Conjugate. HSA-$(MORF2)_x$ conjugate was synthesized by maleimide functionalization of human serum albumin (HSA) surface followed by thiol−ene reaction with thiol modified MORF2.[10] Briefly, HSA (3.35 mg, 50 nmol) was dissolved in 450 μL of 10 mM PBS (pH 7.4), and SM-$(PEG)_2$ (2.5 mg, 5.5 μmol) was dissolved in 50 μL of dimethyl sulfoxide. Then the two solutions were mixed and the reaction was stirred for 2 h at room temperature to convert the surface amino groups of HSA to maleimide groups. Afterward, unreacted SM-$(PEG)_2$ was removed by ultracentrafiltration (Ultracel 30 000 Da MWCO, Millipore) with 10 mM PBS (pH 6.5) washing four times to yield maleimide modified HSA. And according to modified Ellman's assay, the amount of maleimide molecules per HSA was ∼33.

To prepare MORF2 with a thiol end group, 3′-disulfide amide-derivatized 25-mer phosphorodiamidate morpholino oligomer MORF2 (5′-TATATTGATTCTCCTTGGCTTACTC-linker-disulfide-3′, MW = 8585 Da, customized and purchased from Gene Tools, Philomath, OR) was reduced with TCEP. Briefly, 3′-disulfide amide-derivatized MORF2 (2.51 mg, 300 nmol) was dissolved in 250 μL of 10 mM PBS (pH 7.4) containing 10 mM TCEP. Then the reaction was incubated at 37 °C for 30 min. Afterward the resultant fragment 4-thiolbutanamide and excessive TCEP were removed by ultrafiltration (3000 Da MWCO) and washed four times with 10 mM PBS (pH 6.5). The freshly prepared thiolated MORF2 (250 nmol) was added into maleimide modified HSA solution in 500 μL of 10 mM PBS (pH 6.5) and the reaction was performed at room temperature for 3 h. For synthesis of HSA-$(MORF2)_x$ with different valences, the feeding molar ratios of [HSA-mal] to [MORF2-SH] were 1:2, 1:10, 1:20, and 1:30. At the end, unreacted MORF2 was removed by ultrafiltration (30 000 Da MWCO) with four times PBS (pH 7.4). To prepare fluorescent-labeled HSA-$(MORF2)_x$-Cy3, the surface amine groups of HSA (3.35 mg, 50 nmol) were reacted with cyanine 3 monosuccinimidyl ester (Cy3-NHS, Lumiprobe, 70 μg, 100 nmol) in 1 mL PBS (pH 7.4) for 2 h at room temperature with the feeding molar ratio of 1:2. The obtained HSA-Cy3 was further purified using a PD 10 column to remove the unreacted dye, then followed above procedures.

Characterizations. An ÄKTA FPLC system equipped with Sephacryl S-100 HR16/60 column (GE Healthcare) eluted with PBS (pH 7.2) was used to monitor the reactions. The MORF content was determined by UV−visible spectrophotometry at 260 nm in 0.1 N HCl (252120 M^{-1} cm^{-1}) and HSA content was quantified by bicinchoninic acid protein assay. The amount of Cy3 and Cy5 was measured by the absorbance at 547 and 650 nm on the UV−vis spectrophotometer (Agilent Cary Bio 400), respectively, and calculated based on the standard curve.

Investigation of Hybridization between OBN-MORF1 and HSA-$(MORF2)_x$. Analysis of the hydrodynamic effective diameters of

DOI: 10.1021/acsnano.9b04868
ACS Nano 2019, 13, 11422−11432

OBN-MORF1 conjugate, HSA-$(MORF2)_{10}$ conjugate and their mixture at 1:1 MORF1-MORF2 ratio (in PBS pH 7.4, room temperature, 10 min) was performed using a Zetasizer Nano ZS90 (Malvern Instruments, UK). Analysis of the hypochromic effect upon MORF1-MORF2 hybridization was performed using NanoDrop (ND-1000 spectrophotometer, TECAN). OBN-MORF1 and HSA-$(MORF2)_{10}$ solutions (PBS, pH 7.4 or 0.1 N HCl) were mixed in different ratios with a constant total MORF (MORF1+MORF2) concentration of 2.5 μM at room temperature. Ten min post mixture, the optical density at 260 nm was recorded. All measurements were performed in triplicate.

Visualization of Biorecognition on Raji B Cell Surface. B-lymphoma cell lines including CD20 highly expressing Raji, Raji-GFP, and CD20 negative DG-75 cells were cultured in RPMI-1640 medium (Gibco) supplemented with 10% fetal bovine serum (FBS) and 1% penicillin-streptomycin. Cells were suspended and cultured in T75 cell culture flasks and incubated at 37 °C in a humidified 5% CO_2 atmosphere.

To visualize the hybridization between of OBN-MORF1 and HSA-$(MORF2)_x$ *via* MORF1-MORF2 biorecognition on Raji cell surface, Raji cells (2×10^5) were first incubated with OBN-MORF1-Cy5 (0.5 μM) for 1 h at 37 °C. Then, cells were washed with cold PBS twice to remove unbound OBN-MORF1-Cy5. Afterward, cells were further incubated with HSA-$(MORF2)_{10}$-Cy3 (0.5 μM MORF2) for 1 h at 37 °C. After washed twice with cold PBS, the cell nuclei were stained with 5 μg/mL Hoechst 33392 (Thermo Scientific) for 5 min. At the end, cells were washed with cold PBS three times, and suspended in PBS in 4 well chambers prior to confocal visualization.

To demonstrate the biorecognition of OBN-MORF1/RTX-MORF1 and HSA-$(MORF2)_x$ on cell surface was CD20 receptor specific, a 1:1 cell coculture of CD20 positive Raji-GFP cells expressing green fluorescence protein and CD20 negative DG-75 cells were consecutively treated with OBN-MORF1-Cy5/RTX-MORF1-Cy5 and HSA-$(MORF2)_{10}$-Cy3. The biorecognition on these different two cell lines were distinguished by GFP expression and analyzed by flow cytometry.

Apoptosis Induction Measurements. Raji cells (2×10^5) were treated with RTX (RTX, 0.5 μM, 1 h → cell culture medium, 24 h), cRTX (RTX-MORF1-Cy5, 0.5 μM, 1 h → HSA-$(MORF2)_{10}$, 0.5 μM MORF2, 24 h), OBN (OBN, 0.5 μM, 1 h → cell culture medium, 24 h), cOBN (OBN-MORF1-Cy5, 0.5 μM, 1 h → HSA-$(MORF2)_{10}$, 0.5 μM MORF2, 24 h), RTX and OBN combination (0.5 μM RTX + 0.5 μM OBN, 1 h → cell culture medium, 24 h), or treated as indicated. Afterward, cells were washed with PBS and stained with Annexin V-FITC and propidium iodide (PI) in dark for 15 min, following the RAPID protocol provided by the manufacturer (Oncogene Research Products, Boston, MA).

Maximum CD20 Binding Assay. Raji cells (2×10^5) were incubated with a series of increasing concentrations (0.1, 1, 10, 100, 1000 nM Fab′) of OBN, RTX, Fab′(OBN)-MORF1 and Fab′(RTX)-MORF1 for 1 h at 4 °C. Then cells were washed and stained with Alexa Fluor 488-labeled secondary antibody (1:200, 1% BSA) for 30 min at 4 °C, prior to flow cytometry analysis.

Evaluation of CD20 Translocation within Lipid Rafts. Raji cells (2×10^5) were treated with Cy5 labeled RTX (0.5 μM, 2 h, 37 °C), cRTX (RTX-MORF1-Cy5, 0.5 μM, 2 h, 4 °C → HSA-$(MORF2)_{10}$, 0.5 μM MORF2, 2 h, 37 °C), OBN (0.5 μM, 2 h, 37 °C), cOBN (OBN-MORF1-Cy5, 0.5 μM, 2 h, 4 °C → HSA-$(MORF2)_{10}$, 0.5 μM MORF2, 2 h, 37 °C). Then cells were washed with cold PBS to remove unbound antibodies. Afterward cells were fixed with 4% paraformaldehyde and stained with Alexa Fluor-555 conjugated cholera toxin B subunit (CTB, 10 μg/mL, Thermo Scientific) at 4 °C for 30 min. Then cells were washed and transferred to 4-well chamber for confocal microscopy imaging.

Evaluation of Calcium Influx. Raji cells (4×10^5), loaded with intracellular calcium indicator Fluo-3AM (5 μM, Thermo Scientific) for 30 min at 37 °C, were suspended in 400 μL cell culture medium (containing 2.5 mM Ca^{2+}), and excited at 488 nm and the emission at 530 nm was measured on flow cytometry. A baseline was obtained for 100 s before the addition of RTX-MORF1 (1 μM) or OBN-MORF1(1 μM). Then the fluorescent intensity was recorded for another 300 s. Afterward, HSA-$(MORF2)_{10}$ (5 μM MORF2) was added into the cell suspension and fluorescence intensity was further recorded for 200 s during the HSA-based conjugate stimulation. The bump in flow cytometry signal indicates the addition of the corresponding conjugates to cell solution. Calcium influx is defined as the rise in calcium concentration after the bump, as compared with the baseline before the bump.

Evaluation of CD20 Cross-Linking and Caspase Activation. Raji cells were pretreated with β-cyclodextrin (2 wt %, 20 min) to deplete lipid rafts or pan caspase inhibitor Z-VAD-FMK (50 μM, 1 h), followed by the treatment with RTX, cRTX, OBN, or cOBN as described above. Apoptosis induction after different treatments was measured by dual staining of Annexin V-FITC and PI, and compared with the corresponding controls that were not pretreated.

Evaluation of Actin Cytoskeleton Remodeling. Raji cells (2×10^5) were treated with cRTX (RTX-MORF1-Cy5, 0.5 μM, 1 h → HSA-$(MORF2)_{10}$, 0.5 μM MORF2, 24 h), cOBN (OBN-MORF1-Cy5, 0.5 μM, 1 h → HSA-$(MORF2)_{10}$, 0.5 μM MORF2, 24 h), or nontreated. Then cells were fixed with 4% paraformaldehyde at room temperature for 10 min, and stained with Alexa Fluor 488 phalloidin (1:200 dilution, Thermo Scientific) to label F-actin at 4 °C for 1 h. Afterward, cells were washed and imaged by confocal microscopy.

Evaluation of Intercell Homotypic Adhesion. Raji cells (2×10^5) were treated with RTX, cRTX, OBN, cOBN as described, or not treated. Then the morphologies of cells were captured by microscopy. In another experiment, approximately half of Raji cells were incubated with Vybrant DiI cell-labeling solution (Thermo Scientific) at 37 °C for 20 min to generate Raji-DiI, and further mixed with the other half of Raji-GFP cells. The cell mixtures were treated as above, and flow cytometry was used to evaluate the aggregation behavior of the cells.

Evaluation of Lysosome Collapse. Type II anti-CD20 antibody-induced cell death is executed by lysosomes which disperse their contents into the cytoplasm and surrounding environment. Thus, lysosomal collapse is a characteristic feature of OBN-induced cell death. To correlate the changes in the lysosomal compartment with cell death, Raji cells (2×10^5) were treated with RTX, cRTX, OBN, cOBN as described, or not treated, followed by labeling with Lysotracker (200 nM, 20 min, 37 °C, Thermo Scientific), prior to flow cytometry analysis.

Evaluation of ROS Production. Raji cells (2×10^5) were treated with RTX, cRTX, OBN, cOBN as described, or not treated. Then cells were treated with 2 mM of 2′,7′-dichlorodihydrofluorescein diacetate (H_2DCFDA, Thermo Scientific) for 30 min at 37 °C. Afterward, cells were washed, resuspended in PBS and allowed for recovery for 20 min at 37 °C. Trypan blue (0.004% w/v) was subsequently added to quench the extracellular fluorescence for 5 min. Then cells were washed and flow cytometry was applied to detect the intracellular ROS.

Investigation of *In Vivo* Therapeutic Efficacy. All animal experiments were performed according to the protocol approved by the Institutional Animal Care and Use Committee (IACUC) of the University of Utah.

8-week-old male NOD/SCID-Rag1$^{null}\gamma^{null}$ (NRG) mice were intravenously injected with 4×10^6 Raji cells in 200 μL PBS *via* the tail vein on Day 0. Raji cells were allowed to develop and disseminate systemically in mice for 10 days. On Day 10, 17, and 24, 100 μL saline, OBN (0.5 nmol), or cOBN (OBN-MORF1, 0.5 nmol → HSA-$(MORF2)_{10}$, 1.5 nmol MORF2, with 5 h interval) were given intravenously to the randomly divided mice groups (n = 5–6). The survival rate of mice was recorded over time. The onset of hind-limb paralysis or over 20% body weight loss was the end point.

After mice were sacrificed, fresh femurs from both hind limbs were purged with 5 mL PBS to obtain bone marrow cells. The cell suspension was passed through a 70 μm nylon strainer, washed with PBS, and incubated with ACK lysing buffer (room temperature, 5 min, Thermo Scientific) to remove red blood cells. After being washed twice with cold PBS, allophycocyanin (APC)-labeled mouse antihuman CD19 antibody (10 μL) and PE-labeled mouse antihuman CD10 antibody (10 μL) (BD Biosciences, San Jose, CA) were added

DOI: 10.1021/acsnano.9b04868
ACS Nano 2019, 13, 11422–11432

to 100 μL single-cell suspension to stain the Raji cells in bone marrow.[23] Cells were incubated for 20 min at 4 °C in the dark, and washed with PBS prior to flow cytometry analysis. Raji cells served as positive control.

ASSOCIATED CONTENT

Supporting Information

The Supporting Information is available free of charge on the ACS Publications website at DOI: 10.1021/acsnano.9b04868.

Characterization of OBN-MORF1 conjugate; Characterization of HSA-$(MORF2)_{10}$ conjugate; SDS-PAGE gel electrophoresis analysis of conjugate hybridization; Comparison of OBN-MORF1 and OBN-$(MORF1)_3$ on apoptosis induction; Characterization of $Fab'_{(OBN)}$-MORF1 conjugate; Flow cytometry analysis of residual Raji cells (human CD10+CD19+) in the bone marrow (PDF)

AUTHOR INFORMATION

Corresponding Authors

*E-mail: jiyuan.yang@utah.edu.
*E-mail: jindrich.kopecek@utah.edu.

ORCID

Yachao Li: 0000-0003-4792-0915
Jindřich Kopeček: 0000-0002-4451-6944

Notes

The authors declare the following competing financial interest(s): J.Y. and J.K. are co-inventors on a pending US patent application (PCT/US2014/023784; assigned to the University of Utah) related to this work. J.K. is Chief Scientific Advisor and J.Y. Scientific Advisor for Bastion Biologics. Otherwise, the authors declare no competing financial interests.

ACKNOWLEDGMENTS

The research was supported in part by NIH grant RO1 GM95606 (to J.K.) from the National Institute of General Medical Sciences, Experimental Therapeutics Program of the Huntsman Cancer Institute, and The University of Utah Research Foundation. We acknowledge support of funds in conjunction with grant P30 CS042014 awarded to Huntsman Cancer Institute.

REFERENCES

(1) Scott, A. M.; Wolchok, J. D.; Old, L. J. Antibody Therapy of Cancer. *Nat. Rev. Cancer* **2012**, *12*, 278−287.

(2) Graves, J. D.; Kordich, J. J.; Huang, T. H.; Piasecki, J.; Bush, T. L.; Sullivan, T.; Foltz, I. N.; Chang, W.; Douangpanya, H.; Dang, T.; O'Neill, J. W. Apo2L/TRAIL and the Death Receptor 5 Agonist Antibody AMG 655 Cooperate to Promote Receptor Clustering and Antitumor Activity. *Cancer Cell* **2014**, *26*, 177−189.

(3) Mannix, R. J.; Kumar, S.; Cassiola, F.; Montoya-Zavala, M.; Feinstein, E.; Prentiss, M.; Ingber, D. E. Nanomagnetic Actuation of Receptor-Mediated Signal Transduction. *Nat. Nanotechnol.* **2008**, *3*, 36−40.

(4) Kaplan-Lefko, P. J.; Graves, J. D.; Zoog, S. J.; Pan, Y.; Wall, J.; Branstetter, D. G.; Moriguchi, J.; Coxon, A.; Huard, J. N.; Xu, R.; Peach, M. L. Conatumumab, a Fully Human Agonist Antibody to Death Receptor 5, Induces Apoptosis *via* Caspase Activation in Multiple Tumor Types. *Cancer Biol. Ther.* **2010**, *9*, 618−631.

(5) Wu, K.; Liu, J.; Johnson, R. N.; Yang, J.; Kopeček, J. Drug-Free Macromolecular Therapeutics: Induction of Apoptosis by Coiled-Coil-Mediated Cross-Linking of Antigens on the Cell Surface. *Angew. Chem.,Int. Ed.* **2010**, *49*, 1451−1455.

(6) Kiessling, L. L.; Gestwicki, J. E.; Strong, L. E. Synthetic Multivalent Ligands as Probes of Signal Transduction. *Angew. Chem., Int. Ed.* **2006**, *45*, 2348−2368.

(7) Zhang, Z.; Eckert, M. A.; Ali, M. M.; Liu, L.; Kang, D. K.; Chang, E.; Pone, E. J.; Sender, L. S.; Fruman, D. A.; Zhao, W. DNA-Scaffolded Multivalent Ligands to Modulate Cell Function. *ChemBioChem* **2014**, *15*, 1268−1273.

(8) Li, L.; Yang, J.; Wang, J.; Kopeček, J. Amplification of CD20 Cross-Linking in Rituximab-Resistant B-Lymphoma Cells Enhances Apoptosis Induction by Drug-Free Macromolecular Therapeutics. *ACS Nano* **2018**, *12*, 3658−3670.

(9) Tjandra, K. C.; Thordarson, P. Multivalency in Drug Delivery−When is it too Much of a Good Thing? *Bioconjugate Chem.* **2019**, *30*, 503−514.

(10) Li, L.; Yang, J.; Soodvilai, S.; Wang, J.; Opanasopit, P.; Kopeček, J. Drug-Free Albumin-Triggered Sensitization of Cancer Cells to Anticancer Drugs. *J. Controlled Release* **2019**, *293*, 84−93.

(11) Aluri, S. R.; Shi, P.; Gustafson, J. A.; Wang, W.; Lin, Y. A.; Cui, H.; Liu, S.; Conti, P. S.; Li, Z.; Hu, P.; Epstein, A. L. A Hybrid Protein−Polymer Nanoworm Potentiates Apoptosis Better Than a Monoclonal Antibody. *ACS Nano* **2014**, *8*, 2064−2076.

(12) Riley, R. S.; Day, E. S. Frizzled7 Antibody-Functionalized Nanoshells Enable Multivalent Binding for Wnt Signaling Inhibition in Triple Negative Breast Cancer Cells. *Small* **2017**, *13*, 1700544.

(13) Zhang, N.; Khawli, L. A.; Hu, P.; Epstein, A. L. Generation of Rituximab Polymer May Cause Hyper-Cross-Linking−Induced Apoptosis in Non-Hodgkin's Lymphomas. *Clin. Cancer Res.* **2005**, *11*, 5971−5980.

(14) Li, H.; Sun, Y.; Chen, D.; Zhao, H.; Zhao, M.; Zhu, X.; Ke, C.; Zhang, G.; Jiang, C.; Zhang, L.; Zhang, F. Synergistic Anti-Tumor Therapy by a Comb-Like Multifunctional Antibody Nanoarray with Exceptionally Potent Activity. *Sci. Rep.* **2015**, *5*, 15712.

(15) Kazane, S. A.; Axup, J. Y.; Kim, C. H.; Ciobanu, M.; Wold, E. D.; Barluenga, S.; Hutchins, B. A.; Schultz, P. G.; Winssinger, N.; Smider, V. V. Self-Assembled Antibody Multimers through Peptide Nucleic Acid Conjugation. *J. Am. Chem. Soc.* **2013**, *135*, 340−346.

(16) Puertas, S.; Batalla, P.; Moros, M.; Polo, E.; del Pino, P.; Guisán, J. M.; Grazú, V.; de la Fuente, J. M. Taking Advantage of Unspecific Interactions to Produce Highly Active Magnetic Nanoparticle- Antibody Conjugates. *ACS Nano* **2011**, *5*, 4521−4528.

(17) Kratz, F. Albumin as a Drug Carrier: Design of Prodrugs, Drug Conjugates and Nanoparticles. *J. Controlled Release* **2008**, *132*, 171−183.

(18) Alduaij, W.; Illidge, T. M. The Future of Anti-CD20 Monoclonal Antibodies: Are We Making Progress? *Blood* **2011**, *117*, 2993−3001.

(19) Tobinai, K.; Klein, C.; Oya, N.; Fingerle-Rowson, G. A Review of Obinutuzumab (GA101), a Novel Type II Anti-CD20 Monoclonal Antibody, for The Treatment of Patients with B-Cell Malignancies. *Adv. Ther.* **2017**, *34*, 324−356.

(20) Seyfizadeh, N.; Seyfizadeh, N.; Hasenkamp, J.; Huerta-Yepez, S. A Molecular Perspective on Rituximab: A Monoclonal Antibody for B Cell Non-Hodgkin Lymphoma and Other Affections. *Crit. Rev. Oncol. Hemat.* **2016**, *97*, 275−290.

(21) Alduaij, W.; Ivanov, A.; Honeychurch, J.; Cheadle, E. J.; Potluri, S.; Lim, S. H.; Shimada, K.; Chan, C. H.; Tutt, A.; Beers, S. A.; Glennie, M. J. Novel Type II Anti-CD20 Monoclonal Antibody (GA101) Evokes Homotypic Adhesion and Actin-Dependent, Lysosome-Mediated Cell Death in B-Cell Malignancies. *Blood* **2011**, *117*, 4519−4529.

(22) Niederfellner, G.; Lammens, A.; Mundigl, O.; Georges, G. J.; Schaefer, W.; Schwaiger, M.; Franke, A.; Wiechmann, K.; Jenewein, S.; Slootstra, J. W.; Timmerman, P. Epitope Characterization and Crystal Structure of GA101 Provide Insights into the Molecular Basis for Type I/II Distinction of CD20 Antibodies. *Blood* **2011**, *118*, 358−367.

DOI: 10.1021/acsnano.9b04868
ACS Nano 2019, 13, 11422−11432

(23) Chu, T. W.; Yang, J.; Zhang, R.; Sima, M.; Kopeček, J. Cell Surface Self-Assembly of Hybrid Nanoconjugates *via* Oligonucleotide Hybridization Induces Apoptosis. *ACS Nano* **2014**, *8*, 719−730.
(24) Herter, S.; Herting, F.; Mundigl, O.; Waldhauer, I.; Weinzierl, T.; Fauti, T.; Muth, G.; Ziegler-Landesberger, D.; Van Puijenbroek, E.; Lang, S.; Duong, M. N. Preclinical Activity of the Type II CD20 Antibody GA101 (Obinutuzumab) Compared with Rituximab and Ofatumumab *In Vitro* and in Xenograft Models. *Mol. Cancer Ther.* **2013**, *12*, 2031−2042.
(25) Janas, E.; Priest, R.; Wilde, J. I.; White, J. H.; Malhotra, R. Rituxan (Anti-CD20 Antibody)-Induced Translocation of CD20 into Lipid Rafts is Crucial for Calcium Influx and Apoptosis. *Clin. Exp. Immunol.* **2005**, *139*, 439−446.
(26) Sezgin, E.; Levental, I.; Mayor, S.; Eggeling, C. The Mystery of Membrane Organization: Composition, Regulation and Roles of Lipid Rafts. *Nat. Rev. Mol. Cell Biol.* **2017**, *18*, 361−374.
(27) Sevcsik, E.; Brameshuber, M.; Fölser, M.; Weghuber, J.; Honigmann, A.; Schütz, G. J. GPI-Anchored Proteins Do Not Reside in Ordered Domains in the Live Cell Plasma Membrane. *Nat. Commun.* **2015**, *6*, 6969.
(28) Li, L.; Yang, J.; Wang, J.; Kopeček, J. Drug-Free Macromolecular Therapeutics Induce Apoptosis *via* Calcium Influx and Mitochondrial Signaling Pathway. *Macromol. Biosci.* **2018**, *18*, 1700196.
(29) Hartley, J. M.; Chu, T. W.; Peterson, E. M.; Zhang, R.; Yang, J.; Harris, J.; Kopeček, J. Super-Resolution Imaging and Quantitative Analysis of Membrane Protein/Lipid Raft Clustering Mediated by Cell-Surface Self-Assembly of Hybrid Nanoconjugates. *ChemBioChem* **2015**, *16*, 1725−1729.
(30) Honeychurch, J.; Alduaij, W.; Azizyan, M.; Cheadle, E. J.; Pelicano, H.; Ivanov, A.; Huang, P.; Cragg, M. S.; Illidge, T. M. Antibody-Induced Nonapoptotic Cell Death in Human Lymphoma and Leukemia Cells is Mediated Through a Novel Reactive Oxygen Species-Dependent Pathway. *Blood* **2012**, *119*, 3523−3533.
(31) Zheng, J. Y.; Tan, H. L.; Matsudaira, P. T.; Choo, A. Excess Reactive Oxygen Species Production Mediates Monoclonal Antibody-Induced Human Embryonic Stem Cell Death *via* Oncosis. *Cell Death Differ.* **2017**, *24*, 546−558.
(32) Hartley, J. M.; Zhang, R.; Gudheti, M.; Yang, J.; Kopeček, J. Tracking and Quantifying Polymer Therapeutic Distribution on a Cellular Level using 3D dSTORM. *J. Controlled Release* **2016**, *231*, 50−59.
(33) Zhang, L.; Fang, Y.; Kopeček, J.; Yang, J. A New Construct of Antibody-Drug Conjugates for Treatment of B-Cell Non-Hodgkin's Lymphomas. *Eur. J. Pharm. Sci.* **2017**, *103*, 36−46.

DOI: 10.1021/acsnano.9b04868
ACS Nano 2019, 13, 11422−11432